INTERNATIONAL JOURNAL FOR NUMERICAL METHODS IN FLUIDS
Int. J. Numer. Meth. Fluids 2005; **49**:959–974
Published online 3 August 2005 in Wiley InterScience (www.interscience.wiley.com). DOI: 10.1002/fld.1035

A preconditioned semi-staggered dilation-free finite volume method for the incompressible Navier–Stokes equations on all-hexahedral elements

Mehmet Sahin*,†

FSTI-IE-LMF, Swiss Federal Institute of Technology, CH-1015 Lausanne, Switzerland

SUMMARY

A new semi-staggered finite volume method is presented for the solution of the incompressible Navier–Stokes equations on all-quadrilateral (2D)/hexahedral (3D) meshes. The velocity components are defined at element node points while the pressure term is defined at element centroids. The continuity equation is satisfied exactly within each elements. The checkerboard pressure oscillations are prevented using a special filtering matrix as a preconditioner for the saddle-point problem resulting from second-order discretization of the incompressible Navier–Stokes equations. The preconditioned saddle-point problem is solved using block preconditioners with GMRES solver. In order to achieve higher performance FORTRAN source code is based on highly efficient PETSc and HYPRE libraries. As test cases the 2D/3D lid-driven cavity flow problem and the 3D flow past array of circular cylinders are solved in order to verify the accuracy of the proposed method. Copyright © 2005 John Wiley & Sons, Ltd.

KEY WORDS: viscous incompressible flow; unstructured methods; iterative methods; cavity flow

1. INTRODUCTION

A primitive variable-based finite volume method is presented for solution of the incompressible Navier–Stokes equations on all-quadrilateral/hexahedral meshes. A semi-staggered grid arrangement is used for the primitive variables. This choice leads to better pressure coupling compared to the non-staggered (collocated) approach while being capable of handling non-Cartesian grids. In addition, it eliminates the need for a pressure boundary condition since it is defined at interior points. Furthermore, the summation of the continuity equation within each element can be exactly reduced to the domain boundary, which is important for the global mass conservation. But the most appealing feature of the method is leading to very simple algorithm consistent with the boundary and initial conditions required by the Navier–Stokes equations. Recently, the semi-staggered arrangement of variables has been used by Rida *et al.* [1], Kobayashi *et al.* [2], Wright and Smith [3], and Smith and Wright [4] for triangular, quadrilateral and hybrid meshes in 2D.

*Correspondence to: Mehmet Sahin, FSTI-IE-LMF, Swiss Federal Institute of Technology, CH-1015 Lausanne, Switzerland.
†E-mail: msahin.ae00@gtalumni.org

Received 18 March 2005
Revised 24 May 2005
Accepted 24 May 2005

Although, the semi-staggered grid arrangement has better pressure coupling it may lead to the checkerboard pressure field particularly on all-quadrilateral/hexahedral meshes. This problem arises when second-order central difference is used for both the continuity and the pressure gradient operator in the momentum equation. Various approaches have been used to overcome this problem. Baliga and Patankar [5] proposed to use unequal-order interpolation. Russell and Abdallah [6] increased the order of the gradient term in the momentum equation and enlarged the stencil for the pressure Poisson equation. Another approach used by Kobayashi *et al.* [2] is based on the reconstruction of pressure field from the converged velocity field with oscillatory pressure. The most common approaches involve the derivation of non-conservative pressure Poisson equation [7–9]. As indicated by Prakash and Patankar [10], unequal-order approximation leads to a very coarse mesh for the pressure and it may not be very accurate. The problem with non-conservative approaches is that high-pressure gradients result in high values of the fourth-order pressure derivatives and thus a significant mass source is generated. In the present paper we propose to use a simple filtering matrix as a preconditioner, which essentially enlarges the stencil similar to that of Russell and Abdallah [6] in order to prevent the checkerboard pressure oscillations. However, this enlargement does not pose any difficulty for coding since it is introduced as a result of preconditioning.

Unlike the previous works in References [1–4] we used all-quadrilateral/hexahedral meshes. Although all-hexahedral mesh generation for a general geometry is still a difficult task compared with other elements such as tetrahedral, pyramid, etc., there are several reasons for using all-hexahedral elements [11]. First, hexahedral meshes perform quite well when local mesh is strongly anisotropic such as boundary layers. Second, they are more accurate and efficient for a fixed number of grid points. In addition, the use of cell-centred discretization with other elements causes the number of unknowns to increase significantly for a same number of mesh points. In fact, this is the case for the pressure term in our semi-staggered discretization. For numerical discretization a second-order accurate finite volume method is used. The resulting system of equations leads to the well known saddle-point problem [12, 13]. Here we used preconditioned iterative solvers based on block factorization, which leads to more robust solution techniques [14–18] compared to SIMPLE, SIMPLER, etc. type decoupled solution techniques. Convergence of these decoupled solution techniques can often be problematic and may even result in nonconvergence.

The present paper is organized as follows: Section 2 provides some details of the present finite volume method with preconditioned iterative solvers and pressure coupling in order to prevent the checkerboard pressure oscillations. In Section 3, the proposed method is applied to the well-known 2D/3D lid-driven cavity problem and the 3D flow past array of cylinders in a square channel. Concluding remarks are provided in Section 4.

2. MATHEMATICAL AND NUMERICAL FORMULATION

2.1. Discretization of governing equations

The governing equation of incompressible viscous flow consists of the incompressible Navier–Stokes equations which may be written in dimensionless form as

$$\frac{\partial \mathbf{u}}{\partial t} + (\mathbf{u} \cdot \nabla)\mathbf{u} + \nabla p = \frac{1}{Re} \nabla^2 \mathbf{u} \tag{1}$$

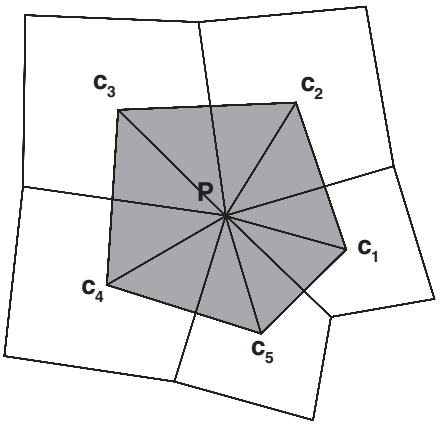

Figure 1. Two-dimensional unstructured mesh with a dual control volume surrounding a node P.

and the continuity equation

$$-\nabla \cdot \mathbf{u} = 0 \tag{2}$$

In these equations, $\mathbf{u}$ represent the velocity vector, p is the pressure and Re is a Reynolds number. Integrating the differential equations (1) and (2) over an arbitrary irregular control volume Ω gives

$$\int_{\Omega} \frac{\partial \mathbf{u}}{\partial t}\,\mathrm{d}V + \oint_{\partial\Omega} (\mathbf{n}\cdot\mathbf{u})\mathbf{u}\,\mathrm{d}S + \oint_{\partial\Omega} \mathbf{n}p\,\mathrm{d}S = \frac{1}{Re}\oint_{\partial\Omega} \mathbf{n}\nabla\mathbf{u}\,\mathrm{d}S \tag{3}$$

$$-\oint_{\partial\Omega} \mathbf{n}\cdot\mathbf{u}\,\mathrm{d}S = 0 \tag{4}$$

The $\mathbf{n}$ represents the outward normal vector, the V is the control volume and the S is the control volume surface area. In the present paper we restricted ourself to the discretization of 2D flows and its extension to 3D is straightforward. Figure 1 illustrates typical four node quadrilateral elements with a dual finite volume constructed by connecting the centroids c_i of the quadrilateral elements which share a common vertex. The discrete contribution from cell c_1 to cell c_2 for the momentum equation is given by

$$\left[\frac{\mathbf{u}_P^{n+1}+\mathbf{u}_1^{n+1}+\mathbf{u}_2^{n+1}}{3\Delta t} - \frac{\mathbf{u}_P^{n}+\mathbf{u}_1^{n}+\mathbf{u}_2^{n}}{3\Delta t}\right] V_{P12} + \left[\mathbf{n}_{12}\cdot\frac{\mathbf{u}_1^{n}+\mathbf{u}_2^{n}}{2}\right]\frac{\mathbf{u}_1^{n+1}+\mathbf{u}_2^{n+1}}{2} S_{12}$$

$$+\mathbf{n}_{12}\frac{p_1^{n+1}+p_2^{n+1}}{2} S_{12} - \mathbf{n}_{12}\frac{\nabla\mathbf{u}_1^{n+1}+\nabla\mathbf{u}_2^{n+1}}{2Re} S_{12} \tag{5}$$

where V_{P12} is the area between the points P, c_1 and c_2, and S_{12} is the length between the points c_1 and c_2. In a similar way other contributions can also be computed. The velocity

vector at the element centroids c_i is computed from the element vertex values using simple averages and the gradient of velocity components are calculated from Green's Theorem:

$$\nabla \mathbf{u}_i = \frac{1}{V_i} \oint_{\partial\Omega_i} \mathbf{n}\mathbf{u}\, \mathrm{d}S \tag{6}$$

where the line integral on the right-hand side of Equation (6) is evaluated using the mid-point rule on each of the element faces. The continuity equation is also integrated in a similar manner within each elements. The discretization of the above equations leads to a saddle-point problem of the form

$$\begin{bmatrix} A_{11} & A_{12} \\ A_{21} & A_{22} \end{bmatrix} \begin{bmatrix} u \\ p \end{bmatrix} = \begin{bmatrix} b_1 \\ b_2 \end{bmatrix} \tag{7}$$

where A_{11} is the convection diffusion operator, A_{12} is the pressure gradient operator and A_{21} is the divergence operator. Here A_{22} and b_2 are zero and $A_{12} \neq A_{21}^{\mathrm{T}}$. Although the system matrix of (7) is indefinite due to zero diagonal block, recent results indicate that indefiniteness of the problem does not represent a particular difficulty and a recent review of the iterative methods for solving large saddle-point problems may be found in References [12, 13].

2.2. *Iterative solvers*

The first approach is the reduction of the saddle-point problem to a Schur complement system, which is based on elimination of the primary unknowns:

$$[A_{21}A_{11}^{-1}A_{12}]\, p = A_{21}A_{11}^{-1}b_1 \tag{8}$$

System (8) is solved by using GMRES [19] with preconditioning which accelerates the rate of convergence of the original problem. Here, we use the approximate Schur inverse preconditioner proposed by Elman [14]:

$$[A_{21}A_{12}]^{-1}[A_{21}A_{11}A_{12}][A_{21}A_{12}]^{-1} \tag{9}$$

This preconditioned iterative solver requires solution of two pressure Poisson and one convection–diffusion subproblems per outer iteration. The solutions of these subproblems are significantly easier to solve than the entire coupled system. Although, the preconditioner first developed by Kay and Loghin and considered further by Kay *et al.* [20] and Silvester *et al.* [21] requires solution of only one pressure Poisson subproblem, it requires construction of other matrices and therefore its application is not straight forward. Additionally, in Reference [15] it is shown that for small time steps Elman preconditioning gives a better rate of convergence.

The second approach is a dual approach that is based on the elimination of the secondary unknown [17, 18]. Here u is expressed as

$$u = [I - A_{12}(A_{21}A_{12})^{-1}A_{21}]u_2 \tag{10}$$

and u_2 is computed from the solution of the following projected system:

$$[I - A_{12}(A_{21}A_{12})^{-1}A_{21}]A_{11}[I - A_{12}(A_{21}A_{12})^{-1}A_{21}]u_2 = [I - A_{12}(A_{21}A_{12})^{-1}A_{21}]b_1 \tag{11}$$

To accelerate the rate of convergence of the above equation we use the inverse of A_{11} as a right preconditioning matrix. As far as the author's knowledge goes this preconditioning is used for the first time in the literature. This preconditioner is based on our numerical experiments which indicated that the coefficients of $A_{12}(A_{21}A_{12})^{-1}A_{21}$ matrix are several orders less than the coefficients of identity matrix I. We solve the above system using GMRES with the preconditioning matrix A_{11}^{-1}, and it also requires solution of two pressure Poisson and one convection–diffusion subproblems. However, the GMRES storage requirement for the dual approach is larger since the velocity vector u_2 is bigger.

Although the preconditioning matrices significantly reduce the number of outer iterations, pressure Poisson and convection–diffusion subproblems need to be solved efficiently. Here, the implementation of the preconditioned Krylov subspace solution algorithm was done using the software package PETSc developed at the Argonne National Laboratory [22]. The preconditioning matrices were obtained from HYPRE developed at the Lawrence Livermore National Laboratory [23]. We used BoomerAMG preconditoner [24] for the pressure Poisson equation and parallel ILU(k) proconditioner [25] for the convection–diffusion subproblem.

2.3. *Pressure coupling*

The semi-staggered discretization of the momentum equations gives all-nonzero pressure coefficients unlike the non-staggered grid arrangement. However, when multiplied with the continuity equation, it produces a pressure Poisson equation with non-zero coefficients only in the diagonal direction as shown in Figure 2(b) for a uniform Cartesian mesh. This kind of operator cannot sense constant pressure field with constant oscillations at diagonal lines and leads to two different pressure fields. A similar problem also exists in the non-staggered case as shown in Figure 2(a). Prakash and Patankar [10] presented four different (odd–odd, even–even, odd–even and even–odd) solutions for the non-staggered grid arrangement. However, the staggered grid arrangements of Harlow and Welch [26] shown in Figure 2(c) can sense these pressure oscillations and lead to unique pressure field. The situation on nonuniform Cartesian meshes is slightly better since nonuniform meshes produce all-nonzero pressure Poisson equation coefficients for the semi-staggered grid arrangement, but still diagonal coefficients are dominant. This coupling may be enough to prevent the pressure oscillations in case pressure field is nonsingular ($p \neq \pm\infty$), such as buoyancy-driven cavity flow, flow past a

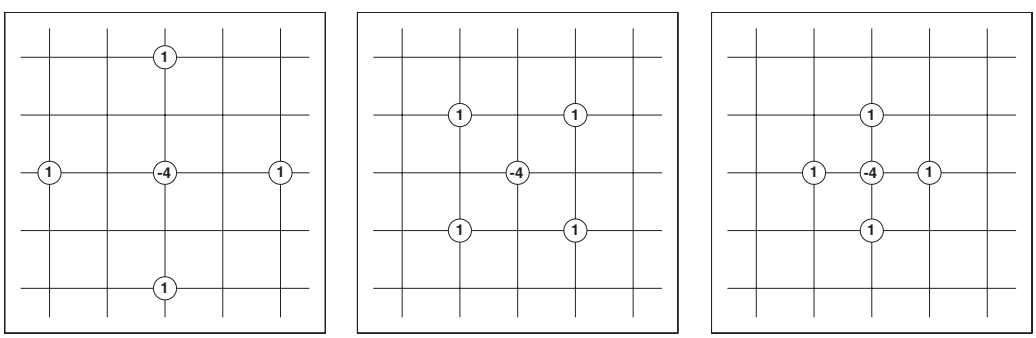

Figure 2. Computational molecules for two-dimensional pressure Poisson equation: (a) non-staggered; (b) semi-staggered; and (c) staggered cases.

circular cylinder, etc., depending on the amount of mesh stretching. Unstructured meshes have better characteristics, but it is difficult to rely on highly nonlinear connectivity information.

In the past, Russell and Abdallah [6] used fourth-order approximation to the pressure gradients in the momentum equations in order to prevent the checkerboard pressure field while satisfying the continuity equations exactly. On unstructured meshes this is a complicated task. In the present paper, we propose to use a simple filtering matrix as a preconditioner, which alters the pressure Poisson equation coefficient weights and enlarges the stencil. The present filtering matrix is based on our numerical observations, which showed that control volume surface pressure values interpolated from element centroids are extremely smooth for the given discretization in Section 2.1. Using this information, we construct control volume surface centre pressure values from the pressure values at element centroids and then reconstruct the original pressure field from the pressure values at control volume surfaces, which is the modified smooth pressure field p^*:

$$p^* = P_{22}\, p \tag{12}$$

Actually, the filtering matrix P_{22} is similar to the restriction operator in the multigrid method. However, the restriction operator is not from fine mesh to coarse one but itself. In 2D half-weighting (HW) and full-weighting (FW) restriction operators can be written in a square mesh as

$$\frac{1}{8}\begin{bmatrix} 0 & 1 & 0 \\ 1 & 4 & 1 \\ 0 & 1 & 0 \end{bmatrix} \text{ (HW)} \qquad \frac{1}{16}\begin{bmatrix} 1 & 2 & 1 \\ 2 & 4 & 2 \\ 1 & 2 & 1 \end{bmatrix} \text{ (FW)} \tag{13}$$

Using the above restriction operators we construct the filtering matrix P_{22} and use it as a preconditioner:

$$\begin{bmatrix} I & 0 \\ 0 & P_{22} \end{bmatrix} \begin{bmatrix} A_{11} & A_{12} \\ A_{21} & 0 \end{bmatrix} \begin{bmatrix} u \\ p \end{bmatrix} = \begin{bmatrix} I & 0 \\ 0 & P_{22} \end{bmatrix} \begin{bmatrix} b_1 \\ 0 \end{bmatrix} \tag{14}$$

Then the modified saddle-point problem becomes

$$\begin{bmatrix} A_{11} & A_{12} \\ A_{21}^* & 0 \end{bmatrix} \begin{bmatrix} u \\ p \end{bmatrix} = \begin{bmatrix} b_1 \\ 0 \end{bmatrix} \tag{15}$$

where $A_{21}^* = P_{22}A_{21}$. To solve the above equations we used the iterative solvers given in Section 2.2, but replaced A_{21} with A_{21}^*. The modified semi-staggered pressure Poisson operators with half-weighting and full-weighting become as in Figure 3. In these computational molecules both odd and even grid points are included. Theoretically, these computational molecules also admit the checkerboard pressure field as in the work of Russell and Abdallah [6]. However, the weights are significantly altered and it seems to be enough to suppress the checkerboard pressure oscillations for the presented numerical results. It may be possible that one can get a dilation free solution without the P_{22} filtering matrix and then use the modified pressure field p^* or reconstruct the pressure field as in Reference [2]. Another approach might be computation of a dilation-free velocity field using the dual approach and then computation of the pressure field from non-conservative pressure Poisson equations.

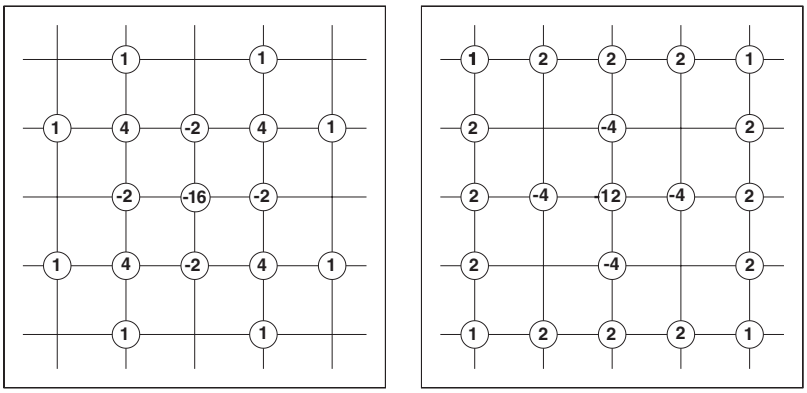

Figure 3. Computational molecules for the semi-staggered two-dimensional pressure Poisson equation with half-weighting (HW) and full-weighting (FW).

3. NUMERICAL EXPERIMENTS

In this section, the proposed method is applied to the well-known 2D/3D lid-driven cavity problem and the 3D flow past array of circular cylinders in a square channel. The present numerical results are obtained by using Euler implicit time marching given in Section 2.1.

The lid-driven cavity problem is well documented in the literature and its detailed description may be found in References [27, 28]. For the 2D lid-driven cavity problem we used both structured and unstructured meshes given in Figure 4. Both meshes have the same number of nonuniform grid points at each cavity edges. The structured mesh consists of 10 201 node points and 10 000 elements while the unstructured mesh consists of 5354 node points and 5153 elements. In order to show the effect of the filtering matrix on the structured mesh, we solve Stokes flow within a square cavity since the pressure at the lower part of the cavity is almost constant and it reveals pressure oscillations easily. The computed pressure field is given in Figure 5 without the filtering matrix and with the filtering matrix. As it may be seen, significant smoothing is achieved with the filtering matrix on the structured mesh. The computed pressure fields are also presented on four different meshes in Figure 6 for the same problem in order to show the effectiveness of the present approach for different mesh resolutions. The present approach seems to be capable of producing smooth pressure fields for all meshes including the coarse one. For the unstructured mesh it may be possible to get a smooth pressure field without the filtering matrix because it is not possible to separate odd and even mesh points from each other due to their highly nonlinear connectivity information. Therefore, unstructured meshes have a tendency to suppress the checkerboard pressure oscillations. However, the connectivity information is highly nonlinear and it is difficult to set *a priori*. A comparison of the computed primitive variables with the filtering matrix is given in Figure 7 for both meshes for the lid-driven cavity flow at $Re = 1000$. Both results are almost same; however, degrees of freedom for the unstructured mesh is significantly lower. For these converged solutions we did not observe any dependency on the time step Δt as expected. For a more accurate comparison, the velocity components are compared at the

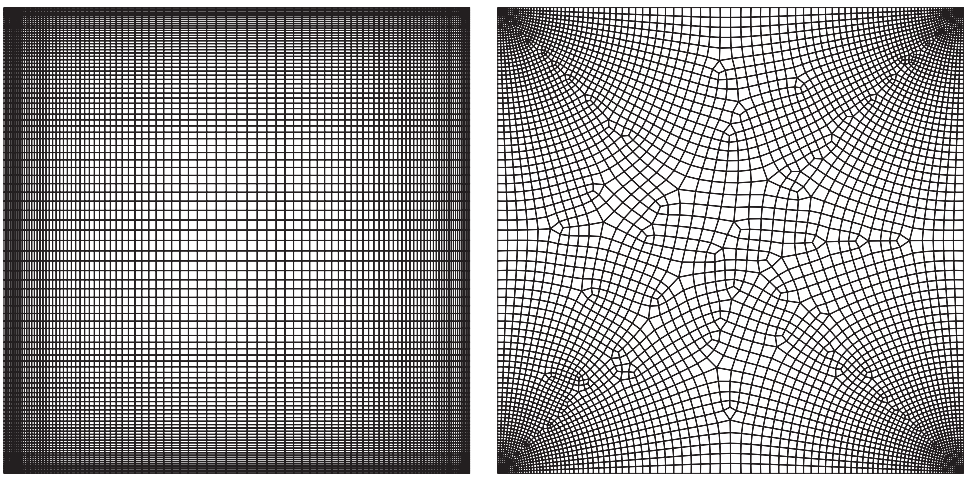

Figure 4. Computational structured (left) and unstructured (right) meshes used for the calculation of the lid-driven cavity problem. The structured mesh: 10 201 node points and 10 000 elements. The unstructured mesh: 5354 node points and 5153 elements.

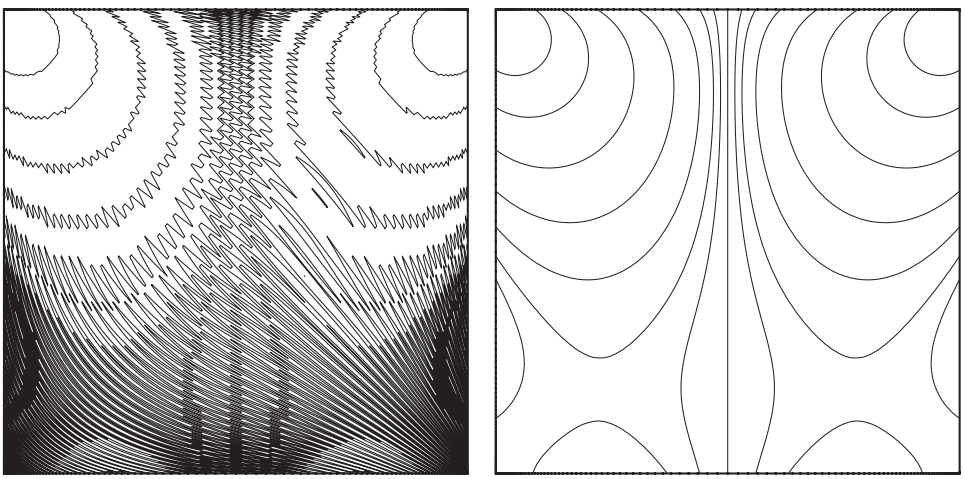

Figure 5. Computed cell centre pressure contours for the lid-driven Stokes flow without the filtering matrix P_{22} (left) and with the filtering matrix P_{22} (right) on the structured mesh.

vertical and horizontal centrelines of the cavity with the results of Ghia *et al*. [27] in Figure 8. The comparison shows good agreement, considering the fact that we have *leaks* at the upper corners. Further improvement is possible using a mesh similar to that of Reference [28].

In addition to our numerical results for the 2D lid-driven cavity problem, we present some results in order to examine the convergence of the preconditioned iterative block solvers given

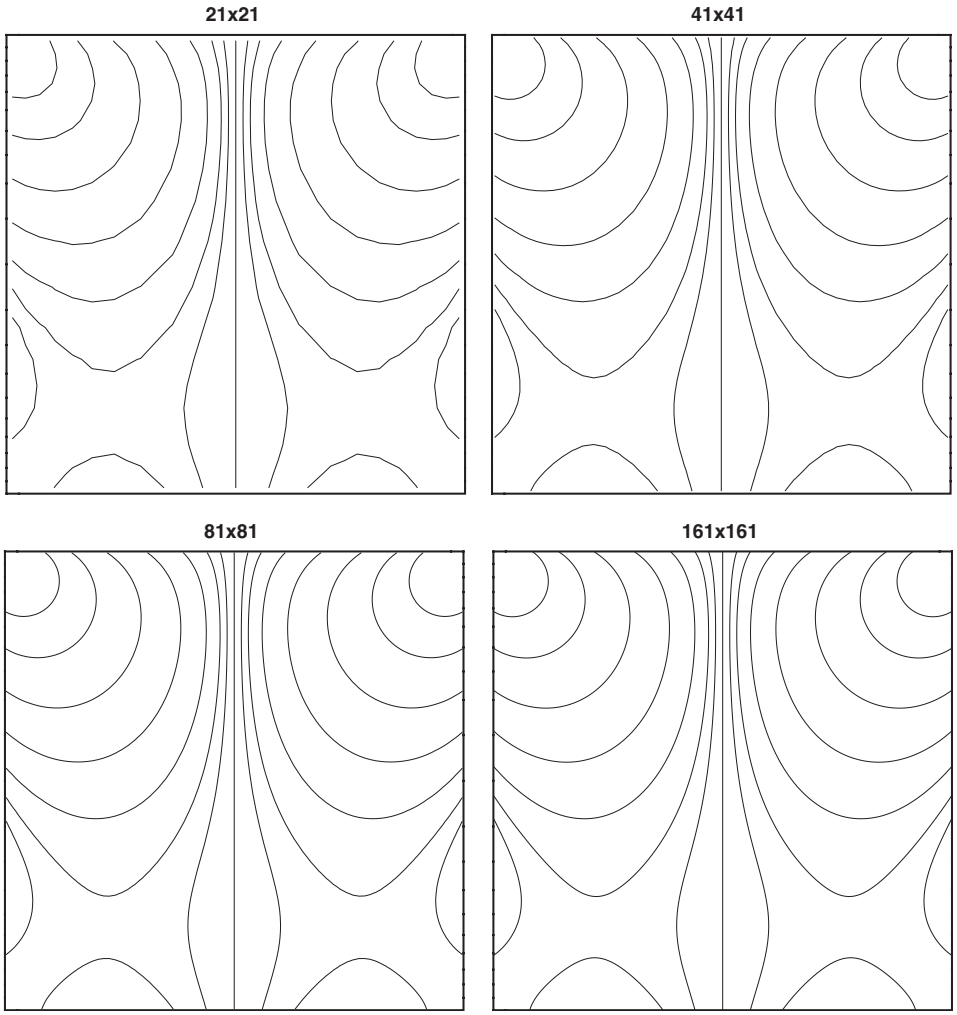

Figure 6. Computed cell centre pressure contours on different meshes with the filtering matrix P_{22} for the lid-driven Stokes flow.

in Section 2.2 at $Re = 1000$. In Table I the required number of outer iterations is given in order to reduce the relative residual to 10^{-8} for the first iteration, which corresponds to Stokes flow, and for the last iteration which corresponds to the converged solution at $Re = 1000$. For these steady-state calculations we found that both methods have similar convergence characteristics. In these calculations the initial solution is set to zero and the number of outer iterations can be significantly reduced by setting the initial solution to the previous outer iteration solution. In Table II the effect of time step Δt to the number of outer iteration is given for several meshes. It seems that there are two limiting values corresponding to $\Delta t \to 0$ and $\Delta t \to \infty$ for each mesh. As the time step decreases the required number of outer iterations are significantly

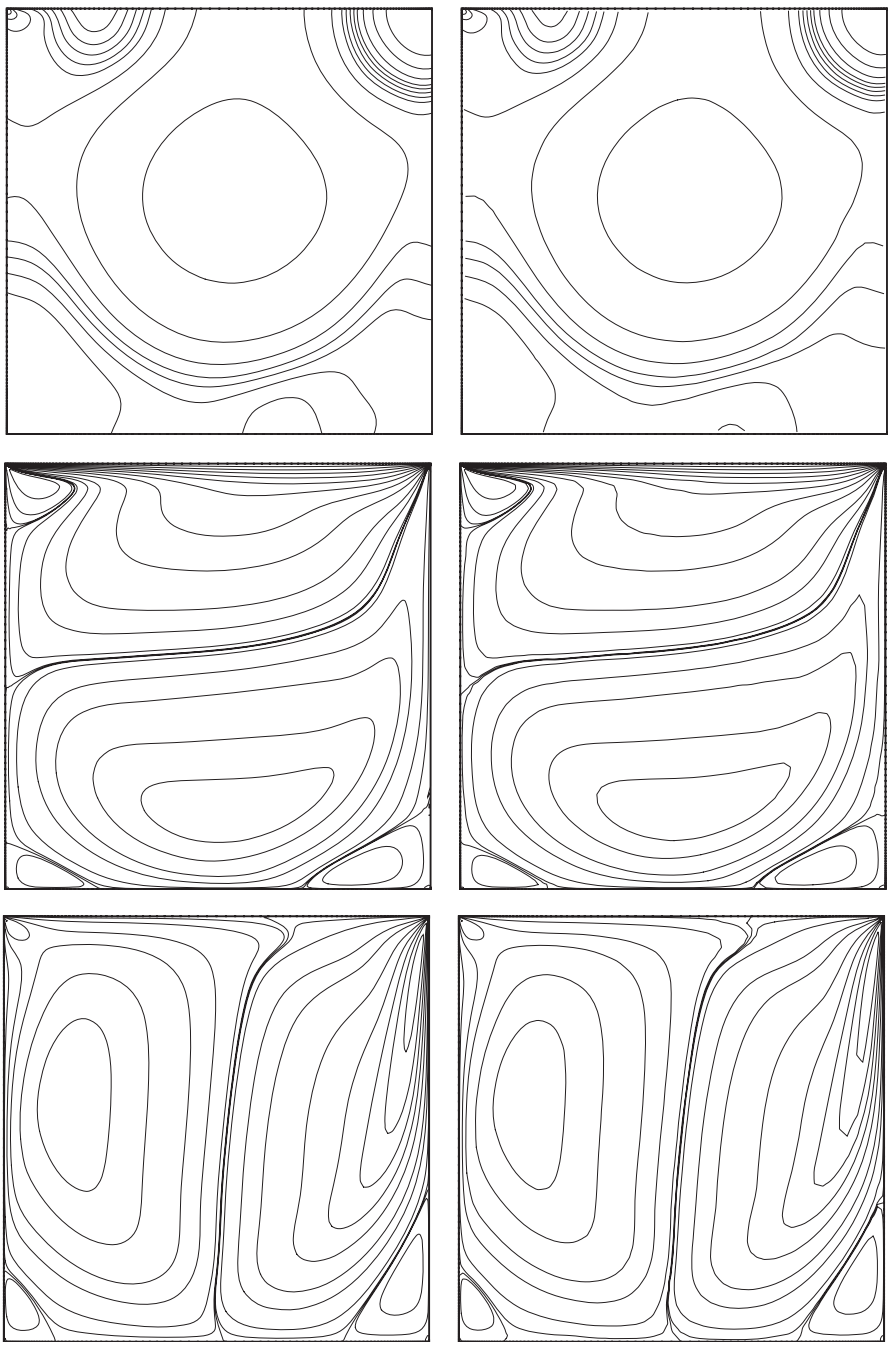

Figure 7. Comparison of computed primitive variables (pressure, u velocity and v velocity) on the structured (left) and unstructured (right) meshes for the lid-driven cavity problem at $Re = 1000$.

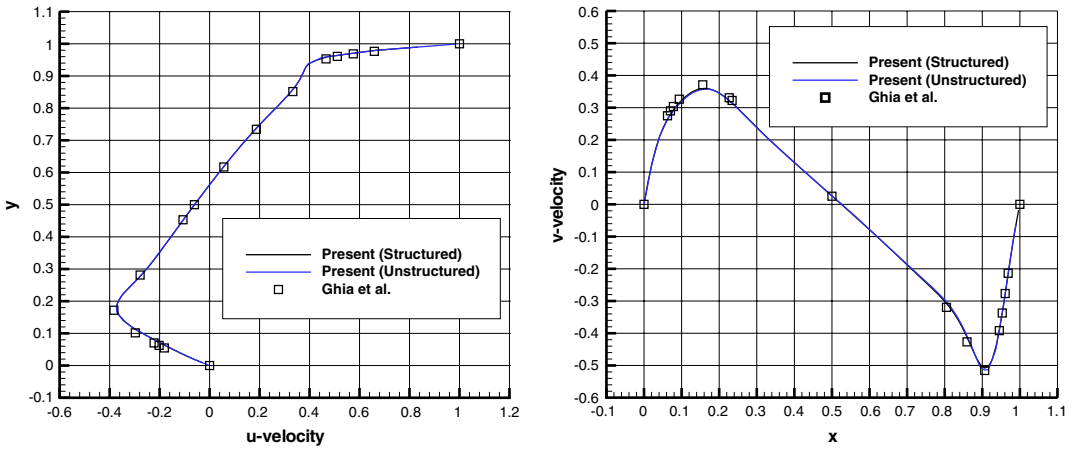

Figure 8. Comparison of computed velocity profiles with the result of Ghia *et al.* [27] through the vertical and horizontal centrelines of the cavity at $Re = 1000$.

Table I. Number of outer iterations for the Schur complement and the dual approach.

	Schur complement		Dual approach	
Mesh	First iteration	Last iteration	First iteration	Last iteration
21×21	10	29	10	31
41×41	13	36	14	37
81×81	17	45	18	49
161×161	22	100	26	108

The first iteration corresponds to Stokes' flow and the last iteration corresponds to the converged solution at $Re = 1000$. The relative residual is 10^{-8}.

Table II. Number of outer iterations for the Schur complement and the dual approach with different time step Δt for the converged solution at $Re = 1000$ on different meshes.

	Schur complement				Dual approach			
Δt	21×21	41×41	81×81	161×161	21×21	41×41	81×81	161×161
10^{-4}	6	6	6	6	6	7	6	6
10^{-3}	6	6	6	6	6	7	6	6
10^{-2}	6	6	6	6	6	6	6	6
10^{-1}	8	8	8	10	8	8	8	10
10^{0}	12	13	15	20	12	14	16	21
10^{1}	24	30	36	58	26	31	37	69
10^{2}	29	35	42	83	30	36	46	96
10^{3}	29	35	45	98	31	37	49	108
10^{4}	29	36	45	100	31	37	49	108
∞	29	36	45	100	31	37	49	108

The relative residual is 10^{-8}.

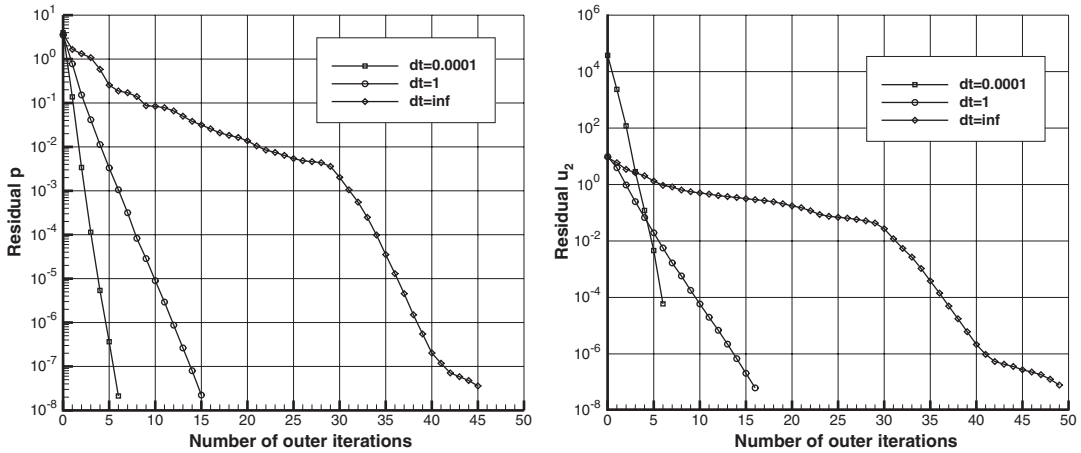

Figure 9. Converge of outer iterations on a 81×81 mesh for the Schur complement (left) and the dual approach (right) with different time step Δt at $Re = 1000$.

reduced and the similarities in the rate of convergence for both methods may be seen in Figure 9 as well. However, we found that the dual approach satisfies the solenoidal velocity constrain better for the same relative residual and this is independent from the number of outer iterations unlike to Schur complement method. In Table III the computed extreme values of $\nabla \cdot \mathbf{u}$ are given as a function of mesh resolution and time step.

The 3D lid-driven cubic cavity problem is solved to establish the reliability and accuracy of the proposed method by way of cross-checking the data against the available three-dimensional results in the literature [29, 30]. Although the geometry is very simple, the flow field can be quite complex. A structured nonuniform mesh with $41 \times 41 \times 41$ node points is used. The present method is also capable of producing smooth pressure field as may be seen from isobaric surfaces in Figure 10. The extreme values of pressure occur at the upper corners, while a low pressure field is observed in the region corresponding to the primary vortex. The computed velocity components along the vertical centreline at $Re = 400$ are compared with the calculations of Jiang *et al.* [29] and as demonstrated in Figure 11, the present numerical results compare well. At this Reynolds number, the three-dimensional computed velocity field is significantly different from the two-dimensional calculations even on the vertical symmetry plane.

A more complex 3D flow past array of circular cylinders in a square channel is also solved in order to demonstrate how well the present numerical method behaves. A computational mesh shown in Figure 12 with 37 180 node points and 31 728 hexahedral elements is used. All the dimensional length scales are nondimensionalized with the cylinder diameter D. The computational domain starts $8D$ upstream of the central cylinder and fully developed flow conditions are imposed using the analytical solutions:

$$u(y,z) = 1.7511 \times \sum_{i=1,3,5,\ldots}^{\infty} (-1)^{(i-1)/2} \left[1 - \frac{\cosh(i\pi z/2H)}{\cosh(i\pi W/2H)}\right] \times \left[\frac{\cos(i\pi y/2H)}{i^3}\right]$$
$$v(y,z) = w(y,z) = 0 \tag{16}$$

Table III. The extreme values of $\nabla \cdot \mathbf{u}$ for the Schur complement and the dual approach with different time step Δt for the converged-solution at $Re = 1000$ on different meshes.

	Schur complement				Dual approach			
Δt	21×21	41×41	81×81	161×161	21×21	41×41	81×81	161×161
10^{-4}	-9.13×10^{-10}	-2.45×10^{-8}	-3.06×10^{-9}	-7.46×10^{-8}	-1.12×10^{-12}	-6.07×10^{-14}	-8.97×10^{-10}	-7.30×10^{-12}
10^{-3}	-9.15×10^{-10}	-5.02×10^{-9}	9.60×10^{-9}	1.59×10^{-7}	-1.12×10^{-12}	-6.85×10^{-14}	-9.16×10^{-10}	-7.24×10^{-12}
10^{-2}	1.09×10^{-8}	-1.37×10^{-7}	7.36×10^{-7}	3.12×10^{-6}	-1.11×10^{-12}	-6.52×10^{-14}	-9.41×10^{-10}	-5.00×10^{-11}
10^{-1}	-5.20×10^{-8}	2.64×10^{-7}	7.78×10^{-7}	2.03×10^{-6}	-1.13×10^{-12}	-7.41×10^{-14}	-1.69×10^{-12}	-8.13×10^{-12}
10^{0}	1.54×10^{-7}	-7.50×10^{-7}	3.67×10^{-6}	1.84×10^{-5}	-6.25×10^{-13}	-2.14×10^{-13}	-1.27×10^{-11}	4.36×10^{-11}
10^{1}	-6.69×10^{-7}	3.43×10^{-7}	5.96×10^{-5}	2.08×10^{-6}	-5.16×10^{-12}	7.07×10^{-13}	-3.96×10^{-11}	-2.81×10^{-10}
10^{2}	1.75×10^{-7}	7.84×10^{-7}	8.56×10^{-7}	3.92×10^{-6}	-8.09×10^{-12}	-1.28×10^{-12}	-5.57×10^{-11}	1.90×10^{-10}
10^{3}	-4.30×10^{-7}	1.59×10^{-6}	1.55×10^{-6}	4.72×10^{-6}	-8.28×10^{-12}	-1.43×10^{-12}	-5.81×10^{-11}	-2.00×10^{-10}
10^{4}	-4.76×10^{-7}	4.17×10^{-7}	1.74×10^{-6}	1.56×10^{-6}	-8.30×10^{-12}	-1.42×10^{-12}	-5.81×10^{-11}	2.92×10^{-10}
∞	-4.86×10^{-7}	4.21×10^{-7}	1.76×10^{-6}	1.64×10^{-6}	-8.26×10^{-12}	1.32×10^{-12}	-5.87×10^{-11}	2.92×10^{-10}

The relative residual is 10^{-8}.

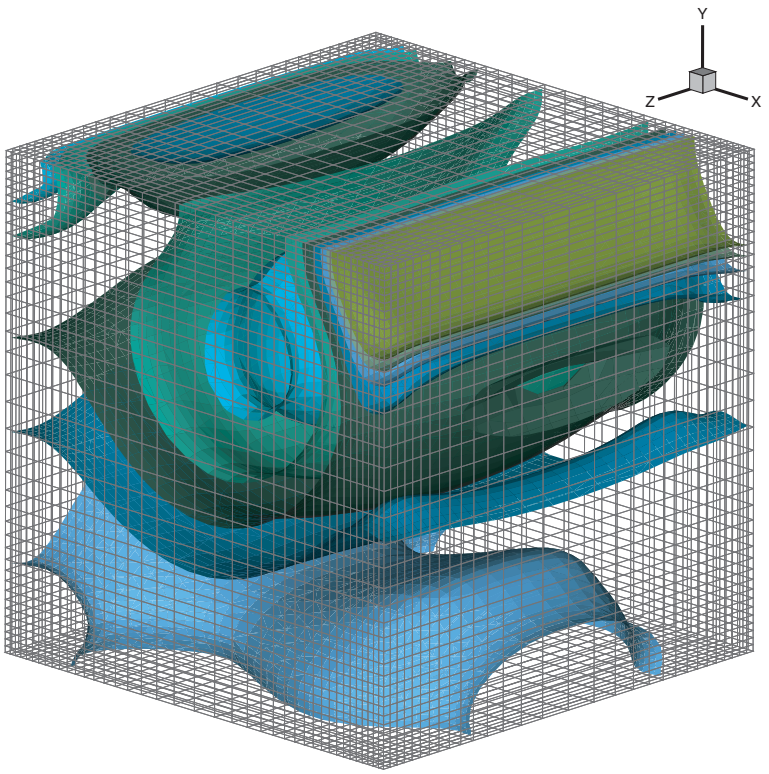

Figure 10. Computed cell centre pressure contours for the lid-driven cubic cavity at $Re = 400$ with a $41 \times 41 \times 41$ mesh.

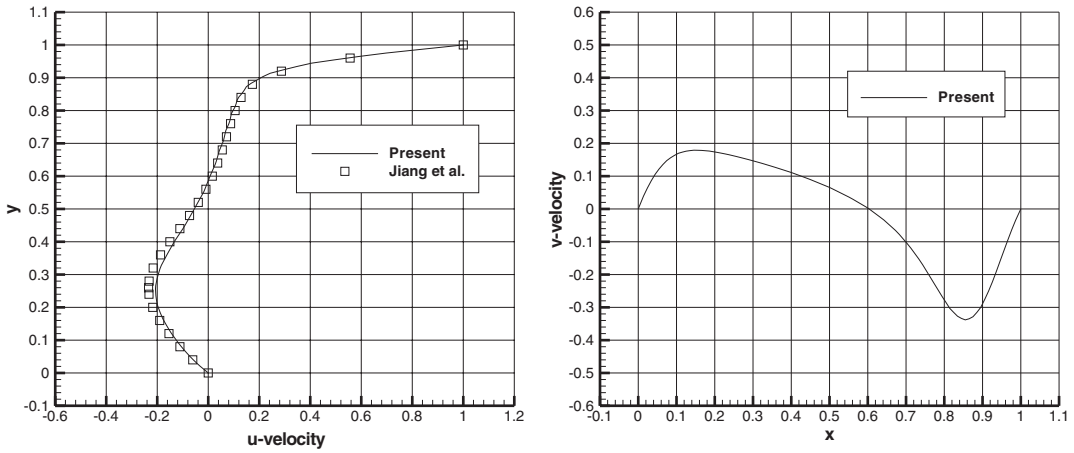

Figure 11. Comparison of computed velocity profiles with the result of Jiang *et al.* [29] through the vertical and horizontal centrelines of the cubic cavity at $Re = 400$.

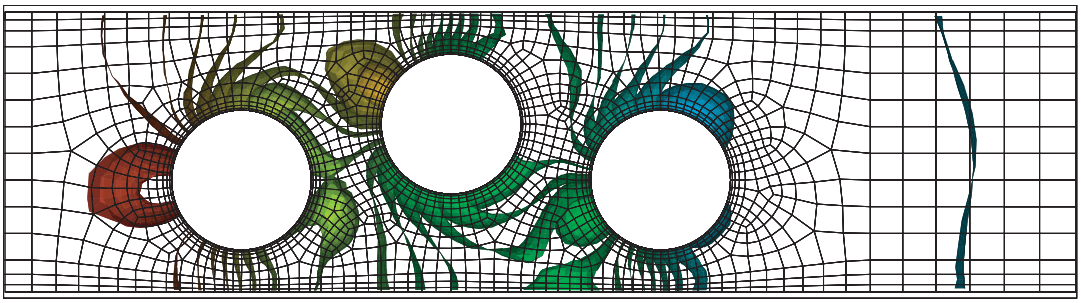

Figure 12. Computed 3D cell centre pressure contours at $Re = 40$ for array of circular cylinders with $D/H = 0.5$ and $H/W = 1.0$.

Here, the maximum inlet velocity is unity. The computational domain ends $20D$ downstream of the central cylinder and outlet boundary conditions are set to natural (traction-free) boundary conditions:

$$\frac{1}{Re}\frac{\partial u}{\partial x} = p, \quad \frac{\partial v}{\partial x} = 0, \quad \frac{\partial w}{\partial x} = 0 \tag{17}$$

On the square channel walls and circular cylinders no-slip boundary conditions are used. The computed cell centre pressure field at $Re = 40$ is given in Figure 12. Although this test case is a rather complex one, the presented isobaric surfaces are smooth.

4. CONCLUSIONS

A new unstructured semi-staggered finite volume method is presented for the solution of the incompressible Navier–Stokes equations with exact mass conservation within each element. The checkerboard pressure oscillations are alleviated using a simple filtering matrix based on linear interpolations. The saddle-point problem resulting from second-order discretization of the incompressible Navier–Stokes equations is solved efficiently using the block preconditioners with GMRES method. The use of highly efficient PETSc and HYPRE libraries allow us to solve a very large system of equations on a single processor and their further testing on multiprocessors is underway for larger problems. The accuracy of the proposed method is verified for the given test cases.

ACKNOWLEDGEMENTS

The author would like to acknowledge simulating discussions with Robert G. Owens at EPFL. The author would also like to thank Dr Barry Smith in PETSc team and Dr Ulrike M. Yang in HYPRE team for their helpful suggestions and comments for coding these libraries.

REFERENCES

1. Rida S, McKenty F, Meng FL, Reggio M. A staggered control volume scheme for unstructured triangular grids. *International Journal for Numerical Methods in Fluids* 1997; **25**:697–717.
2. Kobayashi MH, Pereira JMC, Pereira JCF. A conservative finite-volume second-order-accurate projection method on hybrid unstructured grids. *Journal of Computational Physics* 1999; **150**:40–75.

3. Wright JA, Smith RW. An edge-based method for the incompressible Navier–Stokes equations on polygonal meshes. *Journal of Computational Physics* 2001; **169**:24–43.
4. Smith RW, Wright JA. An implicit edge-based ALE method for the incompressible Navier–Stokes equations. *International Journal for Numerical Methods in Fluids* 2003; **43**:253–279.
5. Baliga BR, Patankar SV. A control volume finite-element method for two-dimensional fluid flow and heat transfer. *Numerical Heat Transfer* 1983; **6**:245–261.
6. Russell PA, Abdallah S. Dilation-free solutions for the incompressible flow equations on non-staggered grids. *AIAA Journal* 1997; **35**:585–586.
7. Rhie CM, Chow WL. Numerical study of the turbulent flow past an airfoil with trailing edge separation. *AIAA Journal* 1983; **21**:1525–1532.
8. Sotiropoulos F, Abdallah S. The discrete continuity equation in primitive variable solutions of incompressible flow. *Journal of Computational Physics* 1991; **95**:212–227.
9. Dormy E. An accurate compact treatment of pressure for collocated variables. *Journal of Computational Physics* 1999; **151**:676–683.
10. Prakash C, Patankar SV. A control volume-based finite-element method for solving the Navier–Stokes equations using equal-order velocity–pressure interpolation. *Numerical Heat Transfer* 1985; **8**:259–280.
11. Tautges TJ. The generation of hexahedral meshes for assembly geometry: survey and progress. *International Journal for Numerical Methods in Engineering* 2001; **50**:2617–2642.
12. Benzi M, Golub GH, Liesen J. Numerical solution of saddle point problems. *Acta Numerica* 2005; **14**:1–137.
13. Rozloznik M. Saddle point problems, iterative solution and preconditioning: a short review. In *Proceedings of the XVth Summer School Software and Algorithms of Numerical Mathematics*, Marek I (ed.), University of West Bohemia Pilsen, 2003, submitted.
14. Elman HC. Preconditioning for the steady-state Navier–Stokes equations with low viscosity. *SIAM Journal on Scientific Computing* 1999; **20**:1299–1316.
15. Elman HC. Preconditioning strategies for models of incompressible flow. *UMIACS-TR-2003-111*, Institute for Advanced Computer Studies, University of Maryland, 2003.
16. Elman HC, Howle VE, Shadid JN, Tuminaro RS. A parallel block multi-level preconditioner for the 3D incompressible Navier–Stokes equations. *Journal of Computational Physics* 2003; **187**:504–523.
17. Amit R, Hall CA, Porsching TA. An application of network theory to the solution of implicit Navier–Stokes difference equations. *Journal of Computational Physics* 1981; **40**:183–201.
18. Hall CA. Numerical solution of Navier–Stokes problems by the dual variable method. *Journal of Computational Physics* 1985; **6**:220–236.
19. Saad Y, Schultz MH. GMRES: a generalized minimal residual algorithm for solving nonsymmetric linear systems. *SIAM Journal on Scientific and Statistical Computing* 1986; **7**:856–869.
20. Kay D, Loghin D, Wathen AJ. A preconditioner for the steady-state Navier–Stokes equations. *SIAM Journal on Scientific Computing* 2002; **24**:237–256.
21. Silvester D, Elman H, Kay D, Wathen AJ. Efficient preconditioning of the linearized Navier–Stokes equations for incompressible flows. *Journal of Computational and Applied Mathematics* 2001; **128**:261–279.
22. Balay S, Buschelman K, Eijkhout V, Gropp WD, Kaushik D, Knepley MG, McInnes LC, Smith BF, Zhang H. *PETSc Users Manual*, *ANL-95/11*, Mathematics and Computer Science Division, Argonne National Laboratory, 2004. http://www-unix.mcs.anl.gov/petsc/petsc-2/
23. Falgout R, Baker A, Chow E, Henson VE, Hill E, Jones J, Kolev T, Lee B, Painter J, Tong C, Vassilevski P, Yang UM. *Users Manual*, *HYPRE High Performance Preconditioners*, *UCRL-MA-137155 DR*, Center for Applied Scientific Computing, Lawrence Livermore National Laboratory, 2002. http://www.llnl.gov/CASC/hypre/
24. Henson VE, Yang UM. BoomerAMG: a parallel algebraic multigrid solver and preconditioner. *Applied Numerical Mathematics* 2002; **41**:155–177. Also available as Lawrence Livermore National Laboratory Technical Report UCRL-JC-141495.
25. Hysom D, Pothen A. A scalable parallel algorithm for incomplete factor preconditioning. *SIAM Journal on Scientific Computing* 2001; **22**:2194–2215.
26. Harlow FH, Welch JE. Numerical calculation of time-dependent viscous incompressible flow of fluid with free surface. *Journal of Computational Physics* 1965; **8**:2182–2189.
27. Ghia U, Ghia KN, Shin CT. High-Re solutions for incompressible flow using the Navier–Stokes equations and a multigrid method. *Journal of Computational Physics* 1982; **48**:387–411.
28. Sahin M, Owens RG. A novel finite volume method applied to the lid-driven cavity problem—Part I: high Reynolds number flow calculations. *International Journal for Numerical Methods in Fluids* 2003; **42**:57–77.
29. Jiang BN, Lin TL, Povinelli LA. Large-scale computation of incompressible viscous flow by least-squares finite-element method. *Computer Methods in Applied Mechanics and Engineering* 1994; **114**:213–231.
30. Ku HC, Hirsh RS, Taylor TD. A pseudospectral method for solution of the three dimensional incompressible Navier–Stokes equations. *Journal of Computational Physics* 1987; **70**:439–462.

